Scars at the edge of the transition from order to chaos in the isomerizing molecular systems LiNC-LiCN and HCN-HNC, and HO_2

F. J. Arranz,[1] L. Seidel,[1] C. G. Giralda,[1,2] R. M. Benito,[1,*] and F. Borondo[3,†]
[1]*Grupo de Sistemas Complejos, Escuela Técnica Superior de Ingenieros Agrónomos, Universidad Politécnica de Madrid, 28040 Madrid, Spain*
[2]*Centro de Investigaciones Energéticas, Mediambientales y Tecnológicas, Avenida Complutense 22, 28040 Madrid, Spain*
[3]*Departamento de Química, and Instituto Mixto de Ciencias Matemáticas CSIC–UAM–UC3M–UCM, Universidad Autónoma de Madrid, Cantoblanco, 28049 Madrid, Spain*
(Received 7 May 2010; published 2 August 2010)

Correlation diagrams of energy levels using $\hbar$ as the varying parameter have proven very useful in the characterization of quantum vibrational dynamics of small polyatomic molecules, specially in relation to the transition from order to chaos. In this paper, we present calculations of such correlation diagrams for three molecular systems with very different characteristics, which can be traced down to the topology of their potential energy surfaces. By studying the broad avoided crossings existing in the diagrams, we show that the transition from regular to irregular states always corresponds to a frontier formed by scarred states.

DOI: 10.1103/PhysRevE.82.026201 PACS number(s): 05.45.Mt, 03.65.Sq, 05.45.Df

I. INTRODUCTION

Last decades have witnessed a tremendous development in the nonlinear science of classical Hamiltonian dynamical systems [1,2]. Particularly important is the Kolmogorov-Arnold-Moser (KAM) theorem [3] on the destruction of invariant tori due to perturbations, which serves as a faithful guide to understand chaotic motion in this kind of systems. In a molecular KAM scenario, the degree of vibrational excitation constitutes a measure of the perturbation leading to chaos. Moreover, the areas of ergodicity created by this mechanism eventually overlap as this perturbation grows, thus giving rise to widespread chaos according to Chirikov's criterium [4].

Molecular dynamics has certainly benefited from such advancement. From the early applications reported in the mid-1980s [5] to the most recent phase space version [6] of the venerable transition state theory, made possible by the importation from celestial mechanics of some sophisticated techniques [7], there have been a wealth of research on the subject [8]. Moreover, the study of the vibrational motions of simple molecules described by realistic potential energy surfaces using the methods of nonlinear dynamics have certainly helped in the understanding of the underlying dynamical processes [9,10], which can be studied by a number of modern experimental techniques [11–13], that go beyond classical molecular spectroscopy [14]. Also, these new methods and their theoretical counterparts [15–17] provide a direct link between spectroscopy and dynamics [18,19].

In molecules, quantum effects are important and they cannot be neglected. These effects when considered in systems whose classical dynamics are chaotic give rise to very interesting phenomena, which constitute the active research field of *quantum chaos* [20,21]. One important development in this area is the so-called scar theory [19,22,23], which studies the influence of periodic orbits (POs) in the eigenfunctions of classically chaotic systems. Heller [25] was the first to find a strong localization of the quantum probability density of certain wave functions along unstable POs in their numerical study of the stadium billiard. This came as an absolute surprise since the opposite to a localization effect was expected [24]. This author also provided a theoretical dynamical explanation for this phenomenon, based on the constructive interference caused by the recurrences produced by the dynamics in the vicinity of the orbits. The hyperbolic structure around the scarring PO is also relevant, as shown in Refs. [26,27]. Finally, another interesting result in scar theory for systems with mixed dynamics, i.e., with regularity and ergodicity coexisting [1,2], was found by Keating and Prado [28,29], who uncover the possibility of superscarring. According to these authors, the localization effect is more pronounced when caused by bifurcating orbits than in the case of isolated ones.

Apart from being scarred, the eigenfunctions of generic dynamical systems may exhibit other topological patterns. Two opposite limits are of interest. First, the integrable or very regular case, in which quantum numbers can be ascribed to the wave function, very much as to what happens in standard textbook examples. In the other limit, we have completely irregular states in which the quantum probability density is, to a high degree, uniformly distributed in configuration and/or phase space, in the spirit of Schnirelman's theorem [24]. Different numerical criteria have been proposed in the literature trying to ascertain the character of a given wave function. Among them, the zeros of the Husimi function [30,31], and the statistics of nodal lines [32] are among the most sensitive ones. However, analyzing the structure of single wave functions except for the case of weak chaos is problematic [22]. The character of otherwise simple structures usually appears strongly mixed, due to eventual complex interactions. However, there is a way to efficiently disentangle these mixtures. It consists of using the correlation diagrams of the corresponding energy levels. Indeed, if the aforementioned structures have different dynami-

*rosamaria.benito@upm.es
†f.borondo@uam.es

cal characteristics, their energies will vary very differently with suitable parameters entering in the Hamiltonian. Accordingly, a simple variation of such parameters should be able to separate the different contributions in a given wave function. As an example, one can vary the value of $\hbar$ to change the relative importance of the kinetic and potential terms, separating in this way the mixtures of harmonic contributions corresponding to different frequencies. This method has been exploited in the past [33–35] in order to analyze the structure of vibrational molecular states.

In correlation diagrams, the Wigner–von Neumann noncrossing rule [36] for states with the same symmetry applies. When two such states evolve as a function of an external parameter, the corresponding energy curves may eventually get very close, but due to this rule they cannot cross. For this reason they are referred to as avoided crossings (ACs), and in the corresponding range of the parameter some mixing of the two involved wave functions takes place. AC's have been shown to be important to understand different dynamical processes in gas [37] and adsorbed phases [38], and also to control [39]. These ACs can be sharp (SACs) or broad (BACs). In the first case, the interaction of states (or alternatively the mixing of their wave functions) is confined to a very narrow range of parameter values, and its net effect is a mere exchange of character, following the simple Landau–Zener model [40]. However, in BACs the interaction is effective in a broad range of values of the parameter, giving rise to the possibility of interacting with many other different eigenstates, the number of which increases, in general, with the density of states. Based on this idea, Marcus *et al.* [41] proposed to use the existence of overlapping BACs as a criterium for quantum chaos, since in this case the topology of the corresponding eigenfunctions would be necessarily complicated.

In this respect, another interesting result is found in Refs. [33,34]. There, it was shown that in the correlation diagram for the LiNC–LiCN isomerizing molecular system a frontier between the regular region, only populated by SACs, and the chaotic region, characterized by the existence of numerous overlapping BACs, could be defined. It actually consisted of a series of isolated BACs, all corresponding to the same quantum resonance [42]. The validity of this conclusion was further assessed by using the Brody exponent (a standard indicator in random matrix theory [43]) which showed a transition from Poisson (regularity) to the Wigner surmise (chaos) in the distribution of nearest neighbors splittings. More interestingly, the interaction taking place in this series of ACs gave always rise to states scarred by the POs corresponding to the above mentioned quantum resonance [34], that were born in this way in the transition from order to chaos taking place at the frontier.

This is an important result, which may have far reaching consequences for molecular systems. A crucial point in this respect is, however, to what extent it can be a general results, applicable to other molecular, or even more general dynamical systems. For this purpose, we extend in this paper our previous work for LiCN to other molecular systems, namely, the HCN molecule and the HO_2 radical, for which some preliminary studies have been performed in our group [44]. We also include, to make the paper complete, a short discussion of the main results found in our previous studies on the correlation diagram for LiNC–LiCN [33,34].

The organization of the paper is as follows. In the next section we briefly describe the molecular systems under study, as well as the computational methods used in our calculations. In Sec. III, we present and analyze some results concerning the correlation diagrams of the vibrational levels of the molecular systems under study. Finally, we summarize our main conclusions in Sec. IV.

II. DESCRIPTION OF THE MOLECULAR SYSTEMS AND CALCULATIONS

A. Molecular systems

In this paper we have chosen three triatomic systems, the LiNC–LiCN and HCN–HNC isomerizing systems, and the HO_2 radical, to perform a comparative study of their correlation diagram of vibrational energy levels. Each of them is characterized by a different topology in their potential energy surface, and the atomic masses of the constituents. However, they share one common characteristic, namely, the vibrational constant of one of their fragments, C–N for LiNC–LiCN and HCN–HNC and O–O for HO_2, is very high, and then the corresponding motion effectively decouples from the remaining modes in the system. Accordingly, the vibrational motion of these systems can be adequately studied with a two degrees of freedom model, where the C–N and O–O distances are kept frozen at their equilibrium values. The corresponding classical vibrational ($J=0$) Hamiltonian is given, in Jacobi coordinates, by

$$H = \frac{P_R^2}{2\mu_1} + \frac{1}{2}\left(\frac{1}{\mu_1 R^2} + \frac{1}{\mu_2 r_e^2}\right)P_\theta^2 + V(R,\theta), \qquad (2.1)$$

where R is the distance from the N–C center of mass to the Li or H atoms for LiNC–LiCN or HCN–HNC, respectively, and the distance from the O–O center of mass to the H atom for the HO_2 radical, r_e is the N–C or O–O equilibrium distance, and θ is the angle formed by the associated vectors.

The potential energy surfaces (PES), $V(R,\theta)$, have been taken from the literature [45–47], and are shown in Fig. 1 as contour plots for the three systems under study. These PESs present for LiNC–LiCN and HCN–HNC two wells at the linear configurations, corresponding to the two existing stable isomers. The most stable one for the first system is the Li–NC ($\theta=180°$), while in the second case the opposite is true, namely, the H–CN ($\theta=0°$) configuration is the most stable. The other two structures, Li–CN ($\theta=0$) and H–NC ($\theta=180°$), are both higher in energy. Moreover, the two isomers are separated in both molecules by moderate energy barriers. The HO_2 radical, on the other hand, has different characteristics, presenting minima at the two equivalent triangular configurations $\theta=46.1°$ and $\theta=133.9°$, respectively. There are also three saddle points, higher in energy, located at $\theta=0,90°$ and 180°, respectively. The first and the last correspond to linear configurations, while the other is at a T–shaped or triangular configuration. The minimum energy paths (MEPs) connecting the different potential wells have also been plotted in dashed line superimposed to the PES.

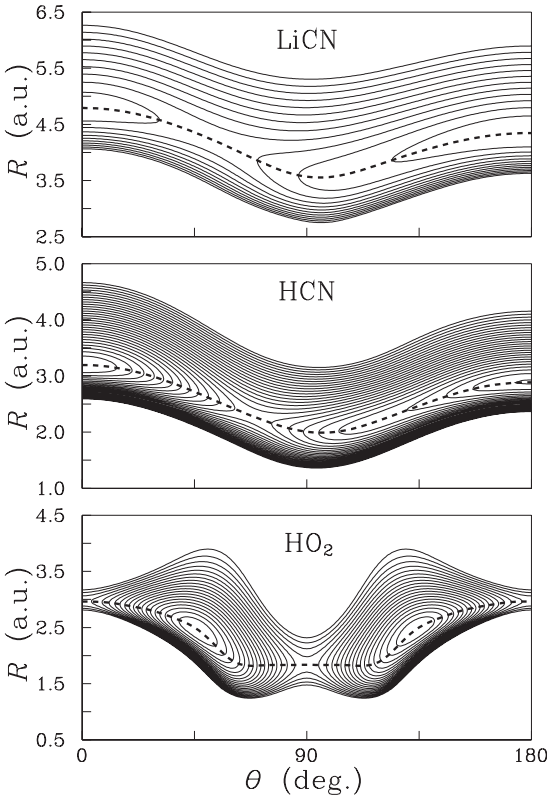

FIG. 1. Potential energy surfaces for the LiNC–LiCN, HCN–HNC, and HO_2 molecular systems. The energy separation between contours is 1000 cm^{-1} in all cases. The minimum energy paths connecting the equilibrium points have also been plotted superimposed in dashed lines.

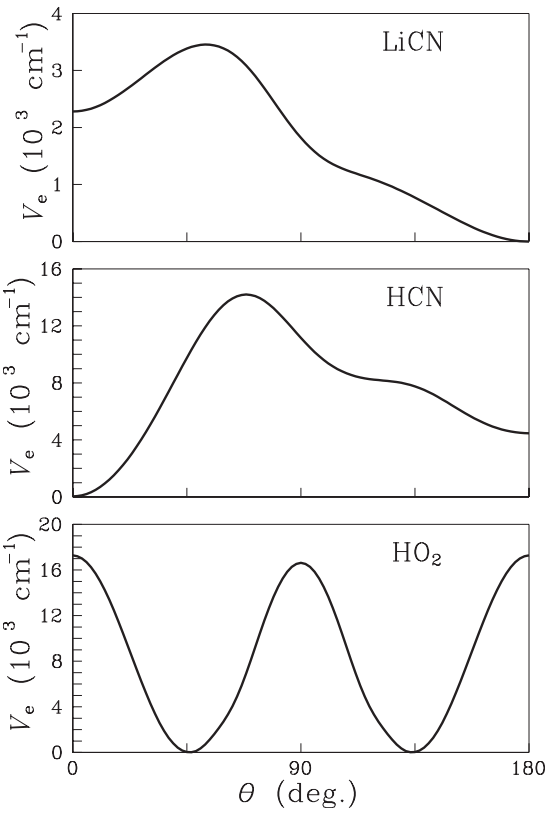

FIG. 2. Potential energy profile along the minimum energy path for the LiNC–LiCN, HCN–HNC, and HO_2 molecular systems.

The energy profiles along the MEPs are shown in Fig. 2 for the three systems. As can be seen, in the first two cases, LiNC–LiCN and HCN–HNC, there is a modest energy barrier at the saddles of the PES separating the two existing stable isomers. For HO_2 we find a symmetric double well potential.

One final point worth commenting is that, due to the characteristics of the PESs, the H, Li or H atoms in LiNC–LiCN, HCN–HNC, or HO_2 can easily perform large amplitude motions in the θ coordinate, thus sampling extensive regions of the corresponding PES, where anharmonicities and intermode couplings are important. This causes that chaos sets in at very low values of the excitation energy in these systems, making them ideal benchmarks for nonlinear science of molecular vibrations.

B. Classical calculations

To follow the dynamics of our three systems we have numerically calculated trajectories using a Gear algorithm to numerically integrate Hamilton equations of motion corresponding to Eq. (2.1). For each trajectory a Poincaré surface of section (SOS) is then computed by taking the MEP, $R_e(\theta)$, connecting the two system isomers (see Fig. 1) as the sectioning surface. In this way, the most significant dynamical information, which is contained in the angular coordinate, is obtained. This choice, however, presents the problem of rendering a SOS which is not an area preserving map. This problem, associated to the fact that the sectioning surface, R_e, depends on one of the coordinates, θ in this case, can be easily solved by making the following canonical transformation [48]

$$\begin{aligned} &\rho = R - R_e(\theta), \quad \vartheta = \theta, \\ &P_\rho = P_R, \qquad\quad P_\vartheta = P_\theta + P_R[dR_e(\theta)/d\theta]. \end{aligned} \tag{2.2}$$

The SOS is now given in these new set of coordinates by the conditions $\rho=0$ and P_ρ being in a predetermined branch (the negative one in our case) of the second degree equation obtained from energy conservation for the momentum. Finally, the data obtained in this way are further folded into the $0 \leq \vartheta \leq \pi$ interval using invariance under the transformation

$$\vartheta \to 2\pi - \vartheta,$$

$$P_\vartheta \to -P_\vartheta, \tag{2.3}$$

to solve, in part, the problem [48] associated with the unphysical (in the sense that the quantum mechanical probability density at the linear configuration is zero [49]) crossing of the $\theta=0$ plane taking place in the classical dynamics [50].

C. Quantum calculations

To perform the quantum mechanical calculations we have used the discrete variable representation-distributed Gaussian basis (DVR-DGB) program of Bačić and Light [51] and

obtained the first 900 vibrational eigenfunctions, $\langle R\theta|n\rangle$, with the corresponding eigenenergies converged to within 0.1 cm^{-1}. However, only the first ~100 low-lying states will be used in the discussions contained in this paper. It should be noted here that due to the symmetric double well character of the PES for HO_2 at low-excitation energies most of the vibrational states considered in the present work will appear degenerate.

Using these data, quantum levels correlation diagrams have been constructed for LiNC–LiCN, HCN–HNC, and HO_2 using $\hbar$ as the actual parameter. The reason for making $\hbar$ variable is simple. As $\hbar$ decreases more and more states can be accommodated in the classical regular region, since the classical dynamics is independent of this parameter. In this way a transition from chaos to order is (artificially) enforced in different states, and their characteristics are then unveiled, as shown previously by us. Also using this method a systematic formation of scars in this system can be observed [34].

III. RESULTS

A. Classical dynamics

Let us examine now the classical dynamics of the systems under study.

1. LiNC–LiCN and the HCN–HNC isomerizing systems

In Fig. 3 we present composite SOSs for LiNC–LiCN at $E=2,500$ cm^{-1}, and for HCN–HNC at $E=11,200$ cm^{-1}. Notice that these energies are high enough to allow the motion of the systems in both of the two existing PES wells, but not to allow isomerizing motion above the barrier. Moreover, it can be observed that in both cases the motion around the well at $\vartheta=0$ is quite regular, taking place on invariant tori. The dynamics on the other well, $\vartheta=180°$, exhibit, on the other hand, mixed regular and chaotic motions. One remarkable feature in the SOS of HCN–HNC is the conspicuous island of regularity found at $\vartheta\simeq 120°$. This is associated to the inflection point that can be seen in the corresponding energy profile along the MEP (see middle panel of Fig. 2), where an adiabatic stabilization of the motion highly excited in the R coordinate takes place [52]. In the LiNC–LiCN system the effect is not so pronounced, but traces of a cantorus [53], with the same dynamical origin, are seen as an accumulation of points next to the LiNC regularity region. In despite of being truly spectacular in their SOS representations, these effects play no role in the issues discussed in the present paper. Another more important fact, since it will be shown to be very relevant for our purposes, is the existence of chains of islands embedded in the chaotic region next to the border of the available energy shell around the second well. They correspond to a 1:8 resonance in the case of LiNC and to a 1:10 resonance for HNC. As it will be shown later, both have a profound influence in the quantum mechanics of the corresponding systems.

2. HO_2 *radical*

Composite SOS for the HO_2 radical are presented in Fig. 4 at three different values of the vibrational excitation energy. Although they look similar to the previous cases, the dynamical characteristics for this system are very different.

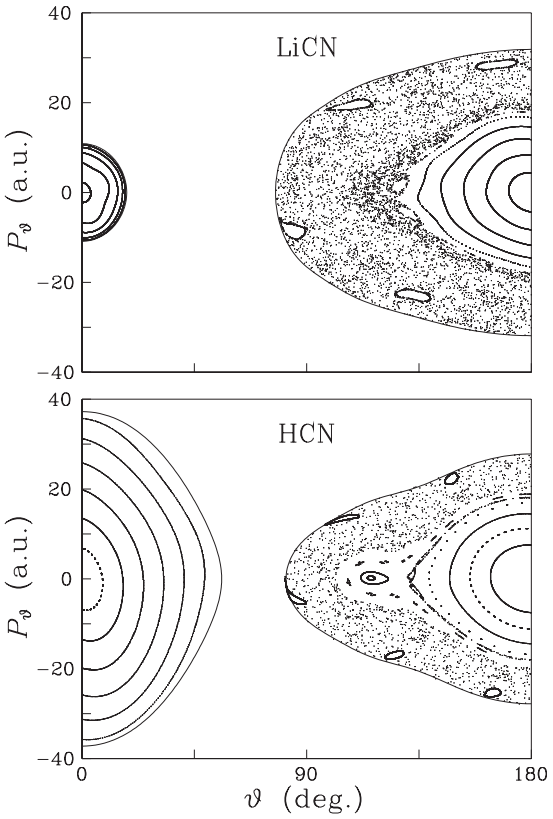

FIG. 3. Composite Poincaré surfaces of section for LiNC–LiCN at a vibrational energy of 2,500 cm^{-1}, and for HCN–HNC at 11,200 cm^{-1}. Notice the existence of a chain of eight islands [taking into account the symmetry of Eq. (2.3)] for LiNC–LiCN and ten in the case of HCN–HNC, close to the energy boundary around the isomers at $\theta=180°$.

As can be observed, at the lowest energy considered, $E=3000$ cm^{-1}, the dynamics are mainly regular, being located the corresponding trajectories in two different regions of the available phase space. The first one is the central region, which appears filled with trajectories confined into invariant tori around the $(\vartheta,P_\vartheta)=(45°,0)$ point. This region is surrounded by a small area of chaos, in which one finds embedded the second region of regularity, formed by a chain of three big islands, which corresponds to a 1:3 resonance. As energy increases, we see at $E=4,500$ cm^{-1}, which is an energy value just of the order of the second excited state, that the central PO becomes unstable, taking place a pitchfork bifurcation that gives rise to a new stable 1:2 PO whose islands of stability are seen in the figure. At the same time, the area of the chaotic region increases substantially, following KAM theorem; the 1:3 chain of islands, however, still survives. Higher up in energy, at $E=12,500$ cm^{-1}, the regular structure in the central part of the SOS has disappeared completely, and new chains of islands appear in the chaotic sea. These islands correspond to stable 1:3 (marked with $\times$) and 1:2 (marked with $\triangle$) POs that are born simultaneously at $E=7,000$ cm^{-1} in a saddle node bifurcation. Two things may seem strange here. In the first place both POs should

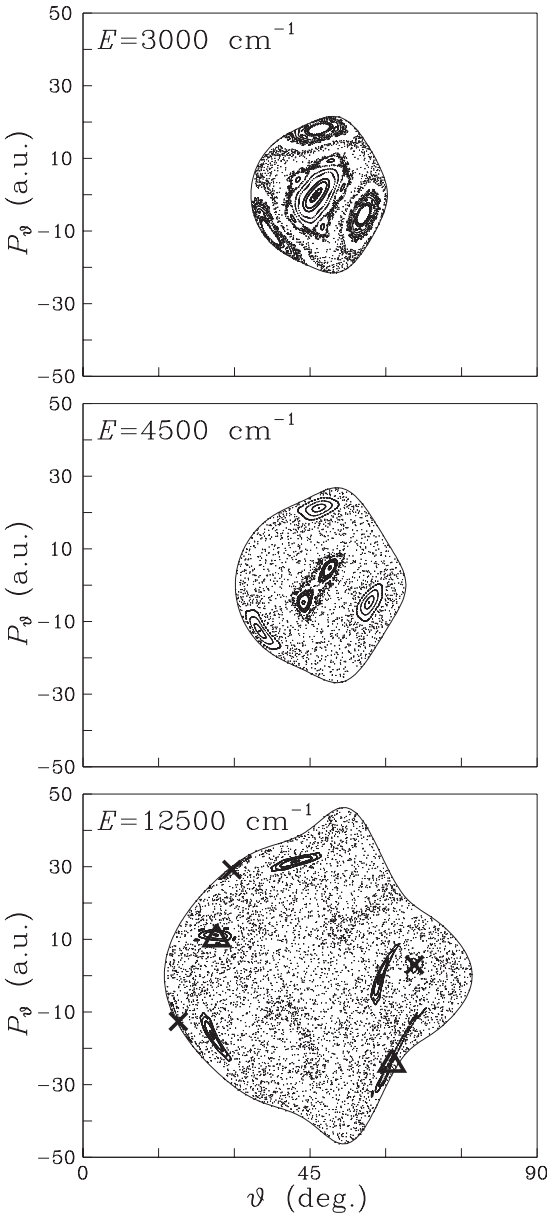

FIG. 4. Composite Poincaré surfaces of section for HO_2 at three values of the vibrational excitation energy. Notice the appearance in the bottom panel of two new chains of islands, corresponding to 1:2 (△) and 1:3 (×) resonances, respectively, which are born in a saddle node bifurcation.

have different stability if born at the same bifurcation, which seems to contradict the fact that both are stable here. What happens is that the 1:2 PO is unstable when born at the bifurcation, but changes later its character at $E > 7{,}000$ cm^{-1}. The second apparent inconsistency is that both POs have different resonance parameter, i.e., 1:3 vs 1:2. Again this is only an unfortunate circumstance, only due to the way in which we calculate our SOS. For molecular systems, taking the MEP as the sectioning plane to compute SOSs provides better dynamical information than any other choice. However, this brings some problems related to the fact that the MEP is not a real trajectory of the system. In our case, and as will be shown later in Sec. III, this makes that these two POs cross a different number of times the SOS, despite the fact that they are dynamically equivalent in every other respect.

B. Correlation diagrams

In this section we will discuss the correlation diagrams of LiCN, HCN, and HO_2, which are presented in Figs. 5–7, respectively.

1. LiNC–LiCN isomerizing system

The correlation diagram of LiCN contains vibrational energy levels up to values of $E/\hbar$ of 4000 cm^{-1}/a.u. This includes, for example, the first 70 eigenvalues corresponding to $\hbar = 1$ a.u. In this plot we have chosen to represent in the vertical axis $E/\hbar$ instead of E to make the figure clearer. The reason for this is the following. At high energies the slope of the energy level curves are very large, and then some portions of the E vs. $\hbar$ plot get too crowded. As a result, some curves get too close to allow for an adequate following of their evolution. This is avoided by using $E/\hbar$ instead of E, since this change progressively reduces the slope of the energy levels curves as $\hbar \to 0$. For example, the low lying states localized in the most stable Li–NC well render horizontal lines (except for very small values of the parameter $\hbar$)

$$\frac{E}{\hbar} = \omega_\rho^{\mathrm{LiNC}}\left(n_\rho^{\mathrm{LiNC}} + \frac{1}{2}\right) + \omega_\vartheta^{\mathrm{LiNC}}\left(n_\vartheta^{\mathrm{LiNC}} + \frac{1}{2}\right), \qquad (3.4)$$

with this choice of scaling, showing their highly harmonic character. On the other hand those states corresponding to the other isomer, Li–CN, appear as hyperbolas displaced vertically

$$\frac{E}{\hbar} = \frac{E_{\mathrm{LiCN}}}{\hbar} + \omega_\rho^{\mathrm{LiCN}}\left(n_\rho^{\mathrm{LiCN}} + \frac{1}{2}\right) + \omega_\vartheta^{\mathrm{LiCN}}\left(n_\vartheta^{\mathrm{LiCN}} + \frac{1}{2}\right). \qquad (3.5)$$

As can be seen in Fig. 5 there are numerous ACs in the correlation diagram of LiCN. However, this number is not uniformly distributed. Indeed, as we consider the region of higher values of E we see that the number of ACs increases and more importantly they are all mostly BACs. As pointed out by Marcus *et al.* [41] this occurrence of many overlapping BACs is a strong indication of mixing of the corresponding wave functions, leading to complex nodal patterns and chaos. On the other hand, in the region of small values of E one only finds SACs. As explained before, at these SACs only a mere exchange of character takes place, thus, being typical of a regular regime. Also, and as discussed in Ref. [34], one can clearly distinguish between these two situations, which appear well separated in the correlation diagram. As a result a frontier between these two situations, chaos and regularity, can be defined. In our case, we have marked the position of this frontier by plotting a series of circles in the diagram along the separation. When this frontier is closely examined, one finds that at the position of each circle there is an isolated BACs. Moreover, the effect of the corresponding interactions is rather peculiar. To illustrate this situation, we show in the rightmost part of the figure the two

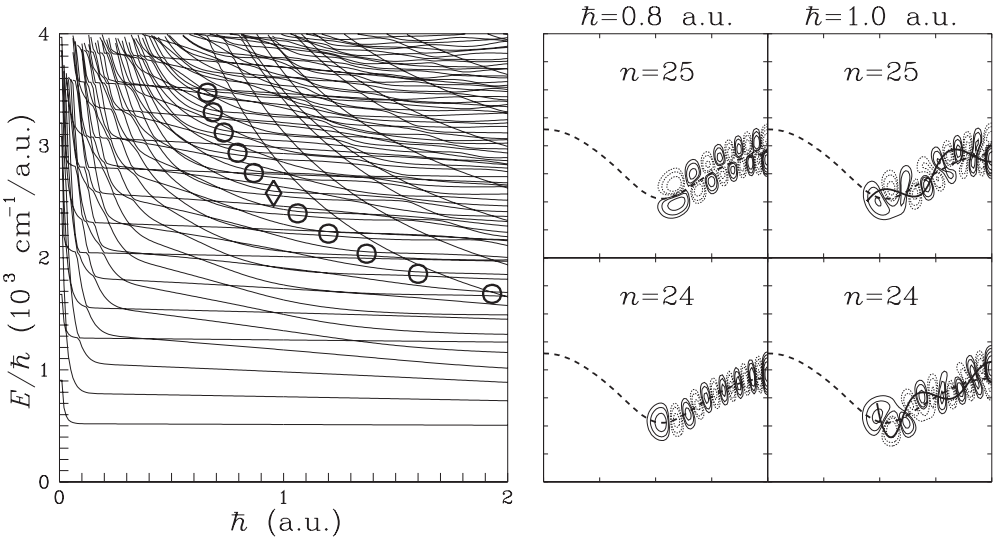

FIG. 5. (Left) Correlation diagram of vibrational energies levels versus $\hbar$ for LiCN. The series of broad avoided crossings that represents the frontier between order and chaos (see text for details) has been marked with circles and diamond. (Right) Wave functions of the states involved in the avoided crossing marked with a diamond in the correlation diagram. The 1:8 periodic orbits corresponding to the chain of islands shown in Fig. 3 have been plotted superimposed in thick line. Also, the minimum energy path has been plotted as a dashed line. The axes in the right panels are the same as in Fig. 1.

wave functions ($n=24$ and $n=25$) involved in the AC marked with a diamond in the corresponding correlation diagram, for two different values of the $\hbar$ parameter. In our case we have chosen the values $\hbar=0.8$ a.u. and $\hbar=1.0$ a.u., which mark positions clearly before and after the AC under consideration. As can be seen in the left column, the wave functions of the interacting states present, before the AC, a regular character with clear nodal patterns along the MEP (also plotted in the figure) and the direction perpendicular to it. The corresponding quantum numbers, $(n_\rho,n_\vartheta)_{\mathrm{LiNC}}=(0,24)$ and (1,16), can then be easily ascribed. Moreover, the difference in these values, $|\Delta n_\rho|:|\Delta n_\vartheta|=1:8$, shows that they are linked by a 1:8 quantum resonance. The situation after the AC is passed is shown in the second column. There, it is clearly observed that the states have changed their characters dramatically, appearing strongly scarred by the 1:8 POs that has been plotted superimposed, which correspond to the unstable ($n=24$) and stable ($n=25$) fixed points in the chain of islands that is visible at the border of the available phase space in the composite SOS on the upper part of Fig. 3. These two orbits are complementary in the sense of the Poincaré–Birkhoff theorem [54], and (as can be seen in the figure) they describe complementary orbits with opposing (inner–outer) turning points. Notice that both classical and quantum resonances responsible for the interactions in this AC are exactly the same.

One final comment concerning the applicability of our correlation diagrams to understanding experiments is in order. Obviously, $\hbar$ cannot be varied in real life. However, varying the value of $\hbar$ in a quantum mechanical calculation

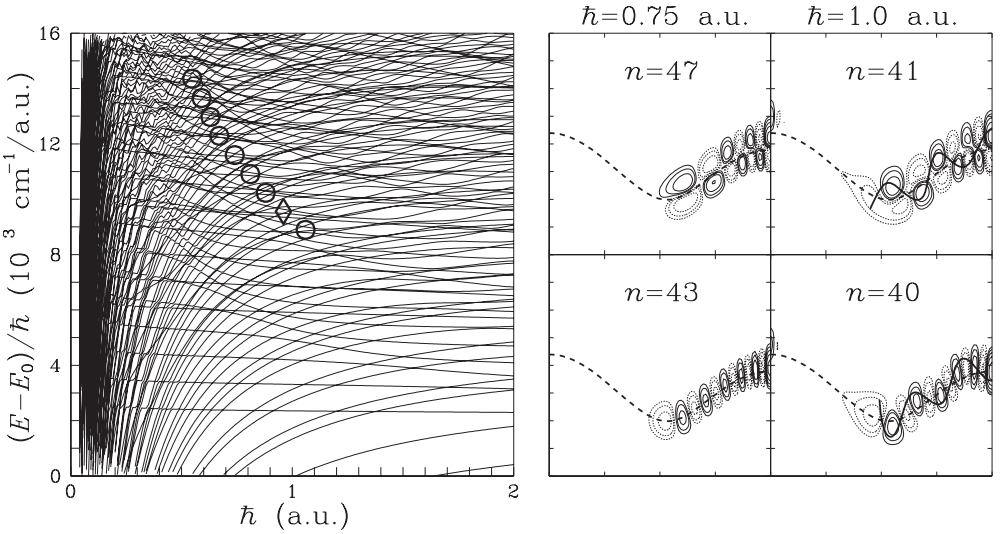

FIG. 6. Same as Fig. 5 for HCN. Here, the zero of the energy scale has been shifted to $E_0=E_{\mathrm{HNC}}$.

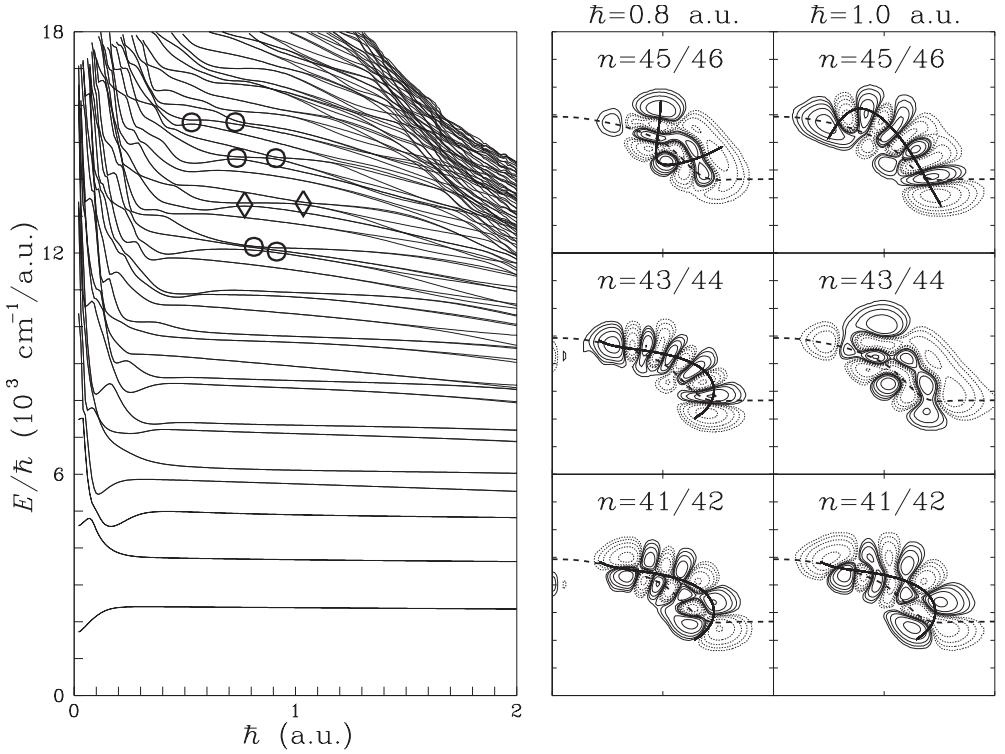

FIG. 7. Same as Fig. 5 for HO_2. Here two series of broad avoided crossings, marked with circles and diamonds, represent the frontier between order and chaos. The range spanned by the horizontal axis in the right panel is $0°-90°$.

is equivalent to scaling all masses of the problem. Although this is strictly not possible in a real molecule due to the reduced number of existing atomic isotopes, at least nature provides us with some combinations. For example, in the present case of the LiNC–LiCN system, instead of the most abundant isotope combination ^{7}Li ^{14}N ^{12}C- ^{7}Li ^{12}C ^{14}N used in the previous calculation, we can use other alternative isotopic substitutions. For example, for ^{9}Li ^{19}N ^{16}C-^{9}Li ^{16}C ^{19}N we have found that the calculated 24th and 25th eigenfunctions (for $\hbar=1$ a.u.) look completely regular and correspond to the states (0,24) and (1,16), respectively.

2. *HCN–HNC isomerizing system*

The situation in the HCN molecule is quite similar, although some differences are present that are worth commenting. In the first place, the correlation diagram which is shown in Fig. 6 is much more crowded, making our study more difficult. Actually, one crucial fact that made possible the identification of the frontier for the order to chaos transition was the shifting of the energy scale by an amount, $E_0=E_{\mathrm{HNC}}$, corresponding to the energy of the HNC isomer. Notice that in this case, we are analyzing the situation taking place around $\theta=180°$ that corresponds to the least stable isomer in the system. One this transformation is done an structure of ACs similar to that for the LiCN case is found, if one takes into account that the curves corresponding to H–CN states are ascendent curves, while the others correspond to the states of the H–NC isomer. The frontier from order to chaos is again indicated with a series of circles plotted in Fig. 6, and as can be seen it marks the transition from mostly SACs to the existence of widespread overlapping BACs. Also, the interaction at the isolated BACs of this frontier produces the formation of scarred states as linear combinations of regular ones. This is illustrated again by showing in the rightmost part of the figure the wave functions involved in the AC marked with a diamond in the correlation diagram. In this case states $(n_\rho,n_\vartheta)_{\mathrm{HNC}}=(0,22)$ and (1,12), linked by a $|\Delta n_\rho|:|\Delta n_\vartheta|=1:10$ quantum resonance, are shown in the left column. The right column shows the corresponding states, scarred by the 1:10 POs whose fixed points correspond to the chain of islands that is visible at the border of the available phase space in the composite SOS on the lower part of Fig. 3.

3. HO_2 *radical*

Let us consider next the case of the HO_2 radical, whose PES is very different from those of the systems that have been discussed before. In Fig. 7 we show the corresponding correlation diagram, in which vibrational levels up to a value of $E/\hbar$ of 18,000 cm^{-1}/a.u. have been plotted. This includes, for example, the first 84 eigenvalues for $\hbar=1$ a.u. Remember that many of the states shown are doubly degenerated, as discussed in Sec. III. As can be seen in the figure, there is a very large region free from chaos for low values of $E/\hbar$ and $\hbar$, similarly to what was found for LiCN. In it, very few ACs, all of the sharp type, are observed, indicating that there are very little interaction among levels. On the other hand, we see that upper right corner gets very crowded since the curves get very close, also having important interactions. This is a consequence of the double well structure presented

by the PES (see lower panels of Figs. 1 and 2). The lowest states are well confined into the wells corresponding to the triangular configurations, and then are very regular. As energy is increased, next and above the barrier, the interaction grows and the states become more complex. Moreover, between these two regions, a series of isolated BACs, which can be identified as forming a frontier between regularity and chaos in this system, are observed. What it is interesting here is that this series of ACs is double, see circles and diamonds in Fig. 7, contrary to what happened in LiNC–LiCN and HCN–HNC. The corresponding interaction is more complex, since it involves three states in each case. Actually, we see that it takes place in two steps. First, two curves approach to later become parallel as $\hbar$ increases. A third party then enter into play avoiding crossing with the two members of the initial pair, this marking the end of the interaction. To understand the net effect of these two processes, we show in the rightmost part of Fig. 7 the wave functions corresponding to the ACs marked with diamonds in the correlation diagram. Just after the first AC ($\hbar=0.8$ a.u.) the two lowest involved states, $n=41/42$ and 43/44 (remember the double degenerate character of these states), appear localized on the 1:3 stable PO plotted superimposed in the figure (see the corresponding fixed points as crosses in the bottom panel of Fig. 4) and characterized by the quantum numbers, parallel and perpendicular to the PO, $(n_{\|},n_{\perp})=(1,6)$ and (0,9), respectively. The third involved state, $n=45/46$, is on the other hand localized on the other unstable 1:2 PO (also plotted superimposed in the figure) originated in the pitchfork bifurcation of the central orbit at $(\vartheta,P_{\vartheta})=(45°,0)$ as described in Sec. II (see transition from the top to medium panels in Fig. 4). Notice that here the two lowest states are also linked by a $|\Delta n_{\|}|:|\Delta n_{\perp}|=1:3$ quantum resonance, as in the previous cases. Once the second AC is passed ($\hbar=1.0$ a.u.) we observe that the net effect of the two interactions is again the formation of scarred states, $n=41/42$ and 45/46. Now, the scarring POs, plotted superimposed to the final wave functions on the last column of the figure, corresponds to the stable 1:3 and 1:2 POs marked respectively with crosses and triangles in the lower panel of Fig. 4.

Finally, let us remark that the main reason for the different behavior observed in this case with respect to LiNC–LiCN and HCN–HNC is that the former presents a non-linear equilibrium geometry. This implies that the couplings leading to chaos are more important. Actually, a similar behavior can be expected in other non linear molecular systems, such as, for example, KCN, which is triangular or the T–shaped He-I_2.

IV. CONCLUDING REMARKS

Modern experimental techniques and theoretical methods allow nowadays the accurate investigation of highly excited vibrational states of small polyatomic molecules. At low energies the corresponding spectra are simple, and the characteristics of the associated states are easily understood by means of standard methods in quantum chemistry. However, for intermediate and high excitations, spectra gets more complex showing new features derived from the different interactions due to anharmonicities and mode couplings. For these cases, different authors have proposed alternative complementary methods that can be used to compute the corresponding states and explain their dynamical characteristics.

In this paper, we extend our previous work on the use of the vibrational levels correlation diagrams to study such excited vibrational states in molecules with classically chaotic behavior. This procedure has been applied here to the study of the low lying states of three floppy triatomic molecular systems, namely, LiNC–LiCN, HCN–HNC and the HO_2 radical, with very different dynamical characteristics. In particular, we have checked our previously obtained conclusion on the scar formation at the edge of the chaotic region [34]. according to which these correlation diagrams can be used to discern the regular and chaotic dynamical regimes at quantum level. And more importantly, the frontier between these two regions is constituted by a series of isolated BACs at which by less or more complicated mechanisms scarred states are formed as combination of regular structures to which definite quantum numbers can be assigned. The new results reported in this paper for the HCN–HNC isomerizing system and the HO_2 radical clearly show that the conclusions drawn by us in Ref. [34] seem to be of general application to the vibrations of molecular dynamical systems.

ACKNOWLEDGMENTS

Support from MICINN–Spain under Contracts No. MTM2006-15533, No. MTM2009–14621, and No. i-MATH CSD2006-32, and Comunidad de Madrid under Contract No. SIMUMAT S-0505/ESP-0158 is gratefully acknowledged.

[1] A. J. Lichtenberg and M. A. Lieberman, *Regular and Chaotic Dynamics* (Springer–Verlag, New York, 1992).
[2] L. E. Reichl, *The Transition to Chaos* (Springer–Verlag, New York, 2004).
[3] V. I. Arnold, A. Weinstein, and K. Vogtmann, *Mathematical Methods of Classical Mechanics* (Springer–Verlag, New York, 1997).
[4] B. V. Chirikov, Phys. Rep. **52**, 263 (1979).
[5] See for example, M. J. Davis, J. Phys. Chem. **92**, 3124 (1988).
[6] C. Jaffé, S. Kawai, J. Palacián, P. Yanguas, and T. Uzer, Adv. Chem. Phys. **130**, 171 (2005)21; T. Bartsch, J. M. Moix, R. Hernandez, S. Kawai, and T. Uzer, *ibid.* **140**, 191 (2008); H. Waalkens, R. Schubert, and S. Wiggins, Nonlinearity **21**, R1 (2008).
[7] S. Wiggins, G. Haller, and I. Mezic, *Normally Hyperbolic Invariant Manifolds in Dynamical Systems* (Springer–Verlag, New York, 1994).
[8] See for example, P. Manikandan, A. Semparithi, and S. Keshavamurthy, J. Phys. Chem. A **113**, 1717 (2009) and the references it contains.

[9] M. Gruebele, Adv. Chem. Phys. **114**, 193 (2000).
[10] J. C. Keske and B. H. Pate, Annu. Rev. Phys. Chem. **51**, 323 (2000).
[11] *Molecular Dynamics and Spectroscopy by SEP*, edited by H. L. Dai and R. W. Field (World Scientific, Singapore, 1995).
[12] D. M. Neumark, Phys. Chem. Chem. Phys. **7**, 433 (2005).
[13] A. H. Zewail, J. Phys. Chem. A **104**, 5660 (2000).
[14] J. M. Hollas, *Modern Spectroscopy* (Wiley, New York, 1996).
[15] F. Iachello and R. D. Levine, *Algebraic Theory of Molecules* (Oxford University Press, Oxford, 1995).
[16] A. G. Csaszar, Spectrochim. Acta, Part A **58**, 599 (2002).
[17] D. Tannor, *Introduction to Quantum Mechanics: A Time-Dependent Perspective* (University Science Books, Sausalito, 2007).
[18] H. S. Taylor, Acc. Chem. Res. **22**, 263 (1989).
[19] E. J. Heller, in *Chaos and Quantum Physics*, edited by M. Giannoni, A. Voros, and J. Zinn–Justin (Elsevier, Amsterdam, 1991).
[20] M. C. Gutzwiller, *Chaos in Classical and Quantum Mechanics* (Springer–Verlag, New York, 1990).
[21] M. V. Berry, Phys. Scr. **40**, 335 (1989).
[22] E. B. Bogomolny, Physica D **31**, 169 (1988).
[23] M. V. Berry, Proc. R. Soc. London, Ser. A **432**, 219 (1989); L. Kaplan and E. J. Heller, Ann. Phys. (N.Y.) **264**, 171 (1998).
[24] A. I. Shnirelman, in *Stochastic Behaviour in Classical and Quantum Hamiltonian Systems*, edited by G. Casati and J. Ford (Springer, Berlin, 1979).
[25] E. J. Heller, Phys. Rev. Lett. **53**, 1515 (1984).
[26] D. A. Wisniacki, E. Vergini, R. M. Benito, and F. Borondo, Phys. Rev. Lett. **94**, 054101 (2005); F. Borondo, E. Vergini, D. A. Wisniacki, A. A. Zembekov, and R. M. Benito, J. Chem. Phys. **122**, 111101 (2005); D. A. Wisniacki, E. Vergini, R. M. Benito, and F. Borondo, Phys. Rev. Lett. **97**, 094101 (2006).
[27] S. Tomsovic and E. J. Heller, Phys. Rev. Lett. **70**, 1405 (1993); Phys. Rev. E **47**, 282 (1993).
[28] J. P. Keating and S. D. Prado, Proc. R. Soc. London, Ser. A **457**, 1855 (2001).
[29] S. D. Prado, E. Vergini, R. M. Benito, and F. Borondo, EPL **88**, 40003 (2009).
[30] P. Leboeuf and A. Voros, J. Phys. A **23**, 1765 (1990).
[31] F. J. Arranz, F. Borondo, and R. M. Benito, Phys. Rev. E **54**, 2458 (1996); F. J. Arranz, R. M. Benito, and F. Borondo, J. Chem. Phys. **120**, 6516 (2004).
[32] S. Gnutzmann, P. D. Karageorge, and U. Smilansky, Phys. Rev. Lett. **97**, 090201 (2006).
[33] F. J. Arranz, F. Borondo, and R. M. Benito, J. Chem. Phys. **104**, 6401 (1996).
[34] F. J. Arranz, F. Borondo, and R. M. Benito, Phys. Rev. Lett. **80**, 944 (1998); J. Chem. Phys. **107**, 2395 (1997).
[35] M. E. Kellman, Ann. Rev. Phys. Chem. **46**, 395 (1995); C. Jung, C. Mejía–Monasterio, and H. S. Taylor, J. Chem. Phys. **120**, 4194 (2004).
[36] L. D. Landau, *Quantum Mechanics Non-Relativistic Theory* (Elsevier, Burlington, 1977).
[37] *The Jahn–Teller Effect*, edited by H. Köppel, D. R. Yarkony, and H. Barentzen (Springer, Berlin, 2009).
[38] A. Gross, *Electronically Non-adiabatic Processes* (Springer, Berlin, 2009).
[39] G. E. Murgida, D. A. Wisniacki, P. I. Tamborenea, and F. Borondo (unpublished).
[40] L. Landau, Phys. Sov. Union **2**, 46 (1932); C. Zener, Proc. R. Soc. London, Ser. A **137**, 692 (1932).
[41] D. W. Noid, M. L. Koszykowski, M. Tabor, and R. M. Marcus, J. Chem. Phys. **72**, 6169 (1980).
[42] F. L. Roberts and C. Jaffé, J. Chem. Phys. **99**, 2495 (1993).
[43] O. Bohigas, J. M. Giannoni, and C. Schmit, Phys. Rev. Lett. **52**, 1 (1984).
[44] L. Seidel, C. González-Giralda, R. M. Benito, and F. Borondo, Int. J. Quantum Chem. **86**, 175 (2002).
[45] R. Essers, J. Tennyson, and P. E. S. Wormer, Chem. Phys. Lett. **89**, 223 (1982).
[46] J. N. Murrell, S. Carter, and L. O. Halonen, J. Mol. Spectrosc. **93**, 307 (1982).
[47] A. J. C. Varandas, J. Brandão, and L. A. M. Quintales, J. Phys. Chem. **92**, 3732 (1988).
[48] R. M. Benito, F. Borondo, J. H. Kim, B. G. Sumpter, and G. S. Ezra, Chem. Phys. Lett. **161**, 60 (1989).
[49] I. N. Levine, *Molecular Spectroscopy* (Wiley, New York, 1975).
[50] J. E. Adams and W. H. Miller, J. Chem. Phys. **67**, 5775 (1977).
[51] Z. Bacic and J. C. Light, Annu. Rev. Phys. Chem. **40**, 469 (1989).
[52] F. Borondo, A. A. Zembekov, and R. M. Benito, Chem. Phys. Lett. **246**, 421 (1995); A. A. Zembekov, F. Borondo, and R. M. Benito, J. Chem. Phys. **105**, 5068 (1996).
[53] T. Geisel, G. Radons, and J. Rubner, Phys. Rev. Lett. **57**, 2883 (1986).
[54] M. V. Berry, AIP Conf. Proc. **46**, 16 (1978).